JOURNAL OF CATALYSIS 124, 160–182 (1990)

Morphologies of Sn and Pt–Sn Phases on Thin Films of Alumina and Graphite

B. E. HANDY,*,[1] J. A. DUMESIC,*,[2] R. D. SHERWOOD,† AND R. T. K. BAKER†,[3]

*Department of Chemical Engineering, University of Wisconsin, Madison, Wisconsin 53706; and †Exxon Corporate Research Science Laboratories, Clinton Township, Route 22 East, Annandale, New Jersey 08801

Received August 28, 1989; revised January 30, 1990

Transmission electron microscopy studies of Sn and Pt–Sn morphologies were conducted on model catalysts, prepared by the vacuum evaporation of metal onto thin films of γ-alumina and sheets of graphite. All supported Sn samples showed nonwetting metallic particles following treatment in hydrogen. Small (<20 nm) particles assumed a core/shell morphology on alumina, due to the existence of a thin oxidic tin–support phase surrounding or beneath a metallic core, whereas the metallic particles on graphite showed uniform contrast. Upon oxidation, metallic Sn particles transformed into toroidal-shaped particles, indicative of an interaction between tin oxide and the substrates. Upon addition of Pt to the supported Sn samples, Pt–Sn alloy formation was observed under reducing conditions. On alumina, the particles were round and surrounded by a light apron. Graphite-supported particles were round and featureless. Upon oxidation of all specimens, the alloy phase was destroyed, as the tin was preferentially oxidized to SnO_2 while the platinum remained metallic, forming a characteristic core/shell appearance. The presence of tin retarded the catalytic oxidation of the graphite substrate by platinum at 770 K. A fraction of the surface tin oxide layer formed during the oxidation treatment of $Pt–Sn/Al_2O_3$ did not re-alloy with the platinum upon reduction, due to interaction with the alumina support.

INTRODUCTION

Platinum-based bimetallics are important materials as petroleum-reforming catalysts. One such patented system is Pt–Sn (*1*). In this system the addition of tin leads to better catalytic stability with enhanced reaction selectivity to higher octane number aromatics when compared to platinum catalysts (*2*). Catalyst behavior has been explained in terms of alloy formation and/or modification of the support by ionic species of the promoter metal (e.g., Refs. (*2–7*)). If alloy particles are formed, then the desired reforming characteristics arise due to surface dilution of active platinum sites by tin, diminishing the number of large platinum ensembles on which coke-forming precursors form. Tin may also modify the electronic nature of active sites and thereby weaken the ability of platinum to adsorb carbon residues, thus moderating the buildup of coke on the active surface. Additionally, tin oxide species may modify the acidic properties of the catalyst support and alter the dispersion of platinum on the support.

The degree of tin reduction has been found to depend on the tin loading, temperature of pretreatment, and presence of surface additives such as chlorine (e.g., Refs. (*2–12*)). For example, Dautzenberg *et al.* (*2*) found evidence for metallic tin at loadings above 0.6 wt%. Oxidic tin surface compounds formed at Sn loadings below 0.6 wt%, but these phases were not reducible. Temperature-programmed reduction of these samples showed a single peak and uptake values consistent with the formation of zero-valent tin at temperatures where

[1] Present address: Dept. Industrial and Engineering Chemistry, Eidgenössische Technische Hochschule (ETH), CH-8092 Zürich, Switzerland.

[2] To whom correspondence should be addressed.

[3] Present address: Department of Chemical Engineering, Auburn University, Auburn, AL 36849.

0021-9517/90 $3.00

platinum could serve as a hydrogen source for Sn species. In Sn/Al_2O_3 catalysts, reduction at 770 K (*4–8*) failed to reduce tin below the +2 state, even for loadings of several percent.

Alloy formation between Pt and Sn is favorable thermodynamically and expected when the metals are in sufficiently close proximity for the tin oxide to accept "spillover" hydrogen from the easily reducible Pt. Indeed, Pt–Sn alloy phases, in addition to oxidic tin states, have been detected from *in situ* studies (*3, 9–11, 13*). In contrast, tin as an oxide could remain dispersed as a thin layer strongly bound to alumina supports, and it can influence reaction behavior by modifying the support acid component.

Electron microscopy is a technique that can be used to determine catalyst morphology and thereby probe the above two limiting models for the Pt–Sn catalyst system. For example, direct observations of a commercial Pt–Sn reforming catalyst by high-resolution electron microscopy have been described by Qiao *et al.* (*14*). Lattice spacings consistent with Pt[001] planes were seen for low tin loadings, and lattice spacings of metallic tin were detected in samples with higher tin contents.

Electron microscopic studies are facilitated by the use of thin film model catalysts, since the observation of individual particles is more distinct on these specimens due to the minimal interference of the support structure on the transmission image (*15*). We report here on the observation of Sn and Pt–Sn morphologies on Al_2O_3 and graphite by transmission electron microscopy following reduction and oxidation at 770 K.

EXPERIMENTAL

Thin films of γ-Al_2O_3 of ca. 10 nm thickness were prepared by anodizing high-purity aluminum foil (Alfa Products, 99.9995%, 0.025 mm thick) in a tartrate buffer solution adjusted to pH 5.5, followed by annealing overnight in oxygen at 870 K (*16*). Sections of the metallic backing were removed for electron microscopic studies of the remaining alumina film by scoring one side of the sample and immersing the strips in a bromine etchant solution. Electron-transparent sheets of a naturally occurring single-crystal graphite (Ticonderoga, NY) were employed for graphite-supported specimens. Half to several monolayers of Pt and Sn were deposited onto the substrates by resistively heating measured amounts of ultrapure Pt and Sn wire (Johnson Matthey, Puratronic Grade) from a tungsten dimple boat under a vacuum of 10^{-5} Torr. Specimen treatments were carried out at atmospheric pressure under flowing gases in a quartz oven.

Transmission electron microscopy (TEM) was conducted with a JEOL 100B instrument operated in bright-field and diffraction modes. The specimens were first reduced in flowing hydrogen at 770 K for 8 h, analyzed, and then oxidized in flowing oxygen at 770 K for 8 h. The same area of the specimen was analyzed between treatments so that the morphological changes of individual particles could be followed. On some specimens, elemental mapping via energy dispersive X-ray analysis (EDX) was performed via scanning transmission electron microscopy (STEM) using a Vacuum Generators HB-501 microscope. A spatial resolution of 2 nm during EDX analysis could be realized, this being determined by the electron beam spot size and beam spreading in the sample.

Controlled atmosphere electron microscopy experiments were performed on selected samples using a JEOL Model 200CX TEM/STEM electron microscope fitted with a gas cell (*17*). The conventional transmission mode was utilized for all studies, for which a point-to-point resolution of 0.8 nm was obtained. Dynamic events were recorded on video tape. Typical runs involved controlled heating specimens in either 3 Torr of oxygen or 1 Torr hydrogen to temperatures up to 1070 K.

The model catalyst specimens are desig-

nated by the metals deposited, in their order of deposition on the substrate, and the substrate material employed, identified as Al_2O_3 for alumina and C for graphite. Additionally, the approximate deposition amount (in monolayers) is given in parentheses. For instance, the designation Pt–Sn (0.5 : 1)/C refers to a sample prepared by evaporating onto a graphite substrate half a monolayer of platinum on top of one monolayer of tin.

RESULTS

Supported Tin Samples: TEM Studies

Tin/alumina. Examination of Sn(10)/Al_2O_3 specimens treated in hydrogen at 870 K showed the presence of two types of particles. Large particles in the size range 50–200 nm have a globular form; however, particles smaller than 20 nm exhibit an unusual morphology: a dense core surrounded by a lighter apron, giving the appearance of a "core/shell" morphology. The electron diffraction pattern of this specimen showed the presence of metallic tin (β-phase).

After subsequent treatment in oxygen at 770 K, both particle types assumed a similar, faceted appearance, as shown in Fig. 1a. At this stage the electron diffraction pattern (Fig. 1b) showed the existence of SnO_2 and SnO, although three moderately strong lines at 0.368, 0.285, and 0.254 nm were present that are not assignable to these phases, and probably represent an intermediate tin oxidation state. Other tin oxide phases have been identified by Asbury and Hoflund (*18*). Thermodynamically, tin should be converted in oxygen to SnO_2 at 500 K. The presence of SnO may represent a stagewise conversion process in the large particles. SnO is normally stable in an inert atmosphere up to 700 K, after which it disproportionates into metallic tin and SnO_2 (*19, 20*).

The nature of the smaller 20-nm tin particles was examined on a specimen prepared with one monolayer of tin. The Sn(1)/Al_2O_3 sample contained particles in the 20- to 30-nm size range after reduction at 770 K. Most of these particles assumed a core/shell morphology, as seen in Fig. 2. The dark center and lighter apron of these particles can be interpreted as a thin oxide layer surrounding or beneath a more electron-dense metallic crystallite core. This morphology can be associated with a particulate metal phase that has been subjected to an oxidation treatment (e.g., Refs. (*21, 22*)). To determine whether core/shell appearance was due to differences in material thickness or to diffraction effects, the specimen was tilted in the electron microscope. The tilting test is important because Bragg diffraction is the primary contrast mechanism, and it can vary considerably with crystallite orientation. Images recorded at 0° and 6.5° tilt did not show any significant changes in contrast.

Images of the same particles following oxidation at 770 K showed a decrease in contrast between the core and the apron, and in some cases the core/shell morphology disappeared. Electron diffraction patterns of the reduced and oxidized Sn(1)/Al_2O_3 specimen indicated that metallic tin was present in the reduced specimen, and conversion to SnO_2 occurred upon oxidation.

Tin/graphite. Model catalysts were prepared with tin loadings of 1 and 10 monolayers. Freshly evaporated tin appeared on both specimens as discrete particles rather than as a uniform metallic layer. The appearance of the untreated Sn(10)/C sample is shown in Fig. 3a. The selected area diffraction pattern of this region showed a spotted ring pattern characteristic of metallic (β-phase) tin. The majority of the freshly deposited tin formed 25- to 50-nm particulates. A network of smaller 10-nm particles is also visible. The bimodal distribution persists even after reduction in hydrogen at 770 K for several hours (see Fig. 3b). The round appearance of the large tin particles suggests that they do not interact strongly with the graphite surface under reducing conditions.

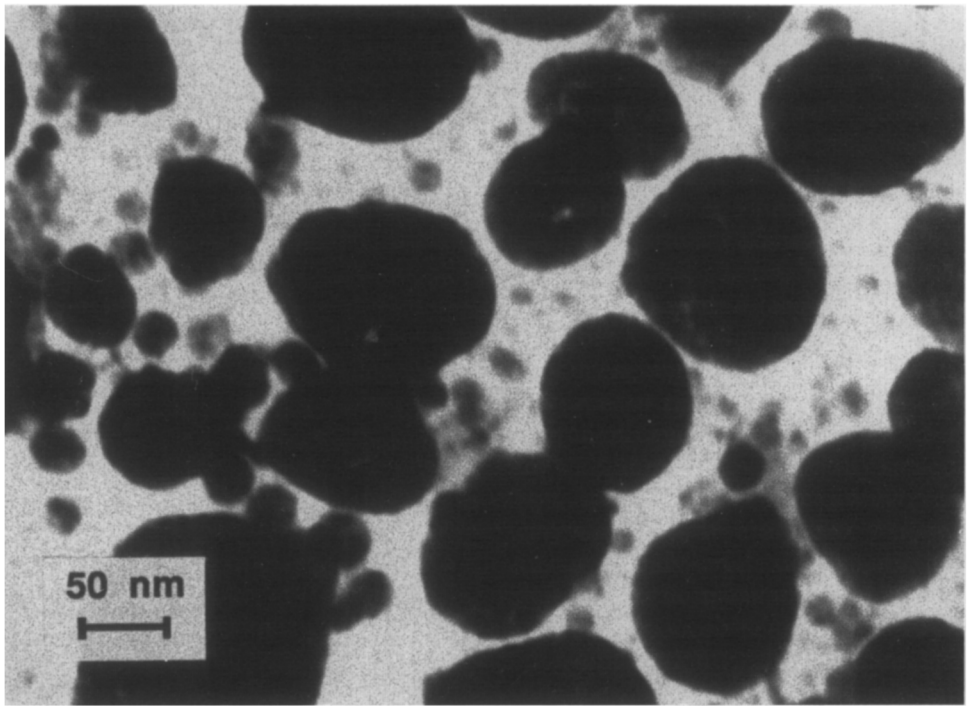

a

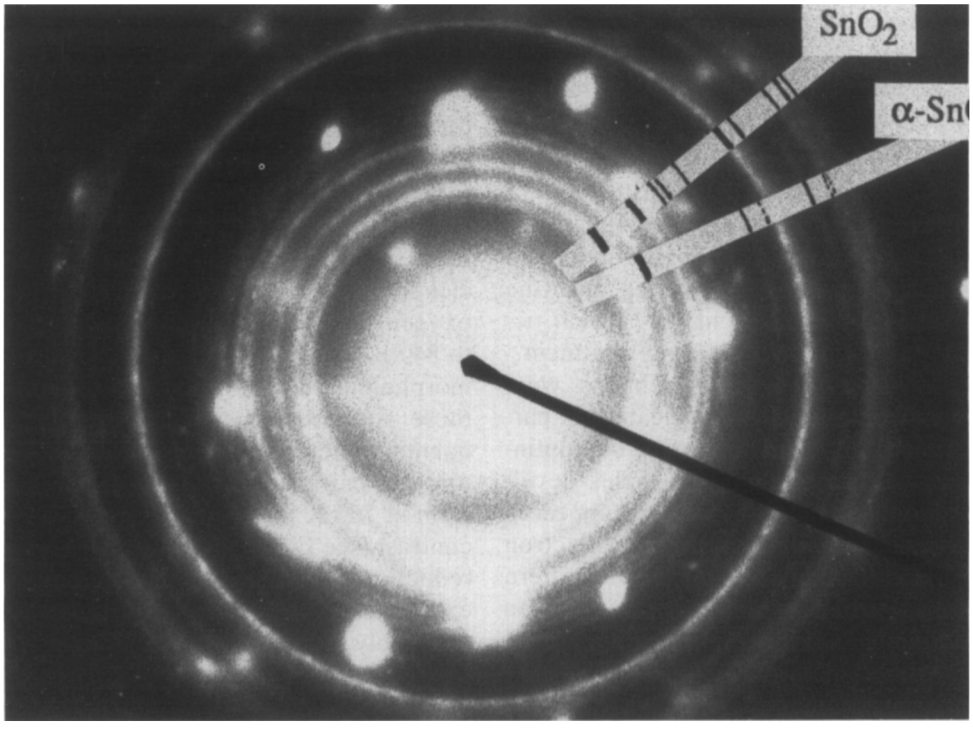

b

FIG. 1. Sn(10)/Al_2O_3 sample oxidized at 770 K for 8 h. (a) Bright field image; (b) diffraction pattern. Spot pattern is from the alumina substrate.

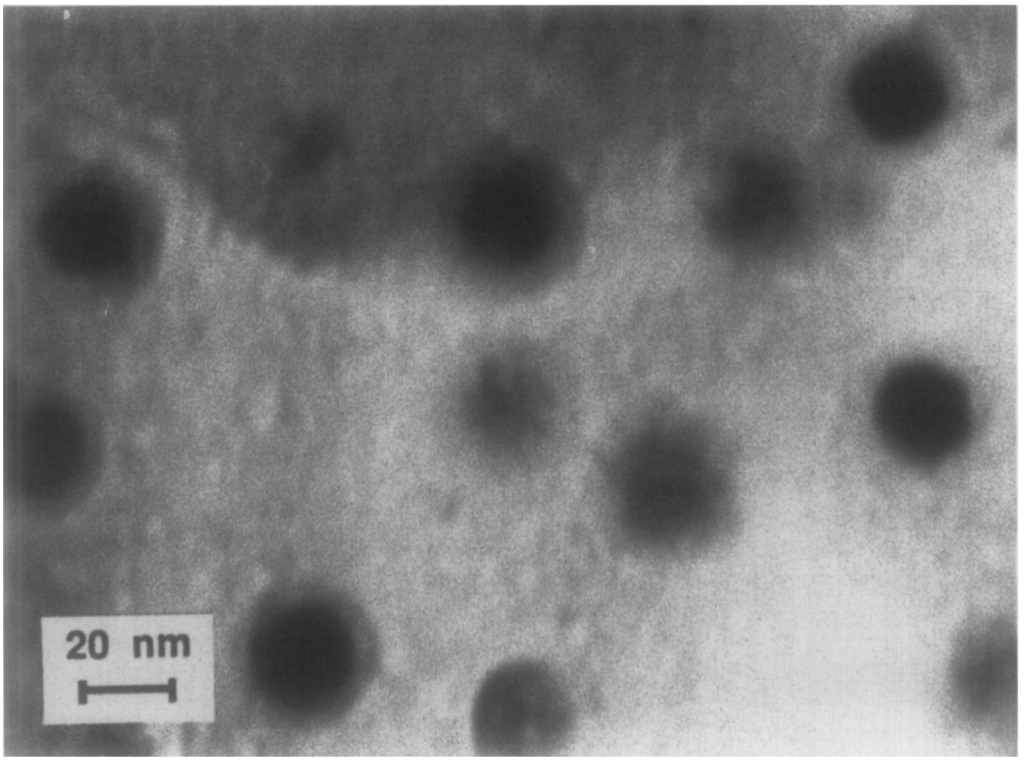

FIG. 2. Bright field image of $Sn(1)/Al_2O_3$ sample reduced at 770 K for 8 h.

Supported Tin Samples: CAEM Studies

It was possible using CAEM to observe directly the appearance of specimens as they were heated in a gas environment and as a consequence gain an insight into the physical and chemical changes which occurred at various stages during treatment.

When $Sn(5–10)/Al_2O_3$ specimens were heated in 3 Torr oxygen, nucleation of particles commenced at 770 K, and on continued heating to 870 K the particles developed a faceted outline and some appeared to have a lighter central region. Electron diffraction examination showed a pattern similar to that obtained from postreaction study of an oxidized tin/alumina specimen (Fig. 1b), with lines corresponding to SnO_2 and SnO. Following oxidation, the specimens were reheated in 1 Torr hydrogen. During this step it was observed that the particle morphology underwent a transformation from a faceted to a smoother outline.

When this sequence of treatments was repeated with specimens containing a lower metal loading, $Sn(1–5)/Al_2O_3$, particle nucleation was detected at 510 K in 3 Torr oxygen, and upon raising the temperature to 840 K most particles assumed a toroidal morphology, as shown in Fig. 4a. When these specimens were cooled and subsequently reheated in 1 Torr hydrogen, the toroidal particles were observed to transform at 760 K into structures with uniform contrast (see Fig. 4b). When this oxidation–reduction cycle was repeated, the particles exhibited the same morphological changes reversibly.

Further CAEM experiments were carried out using a specimen where tin was introduced onto a mixed-support system consisting of overlapping films of alumina and graphite. This type of specimen offers the

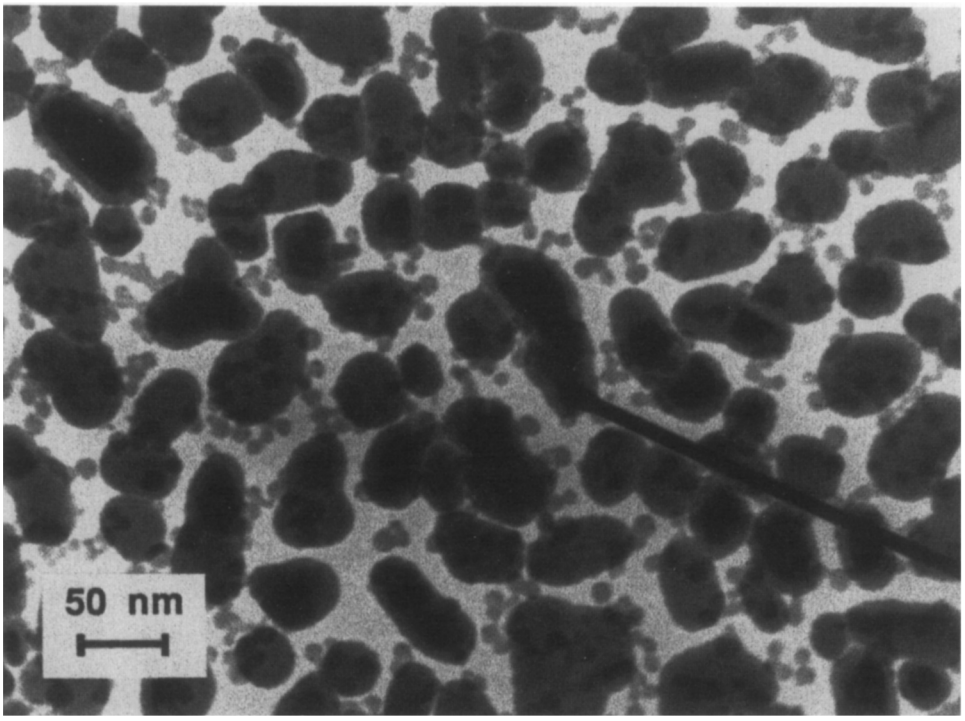

a

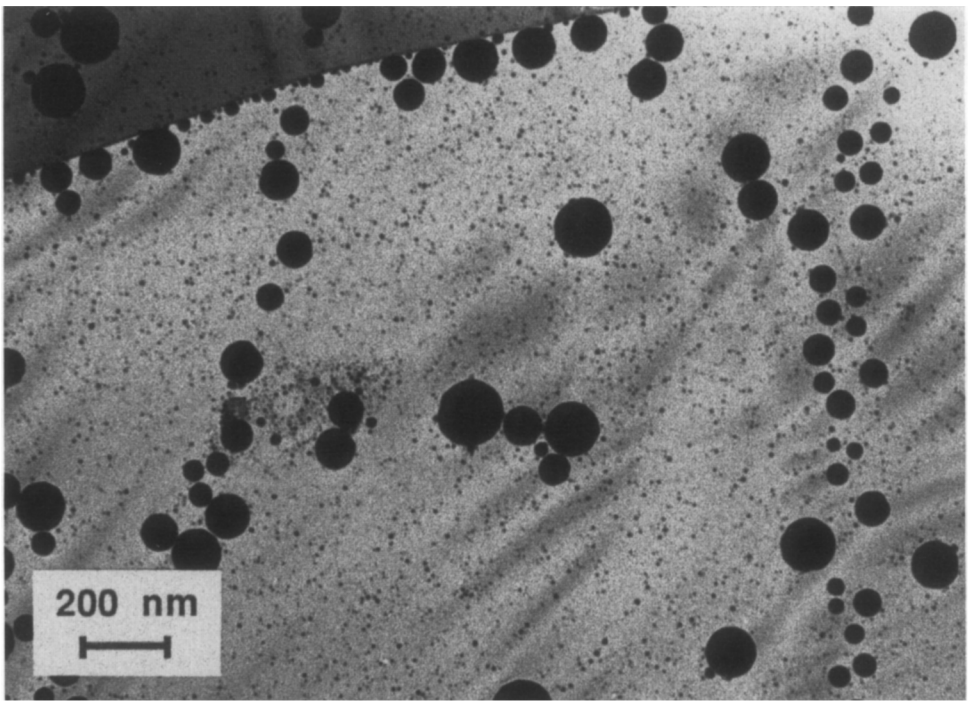

b

FIG. 3. Bright field images of Sn(10)/C sample. (a) After metal deposition; (b) after reduction in hydrogen at 770 K for 8 h.

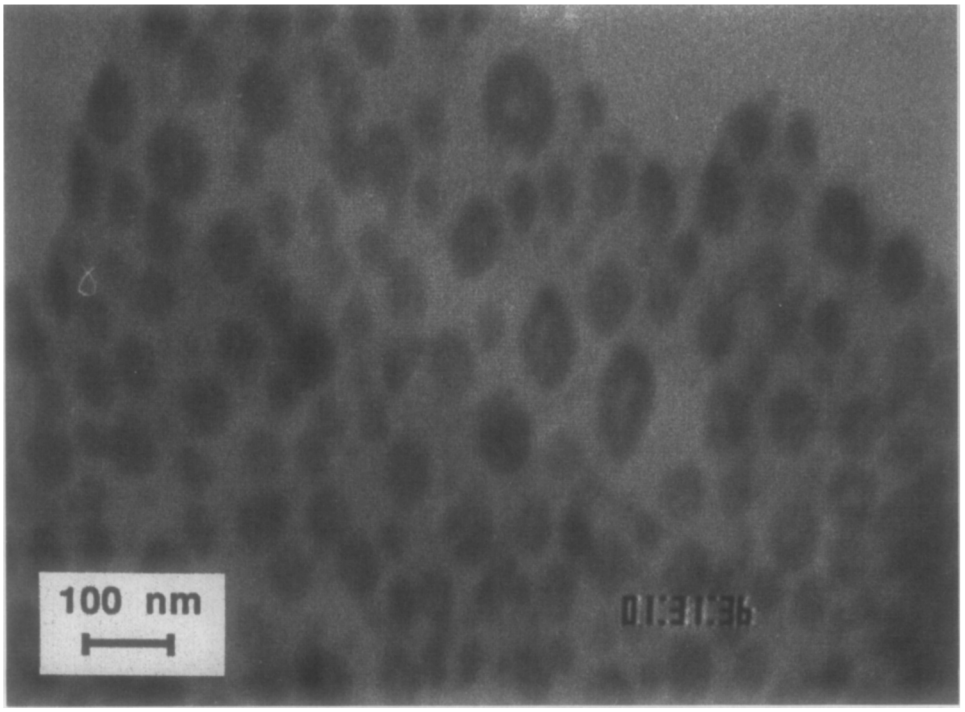

a

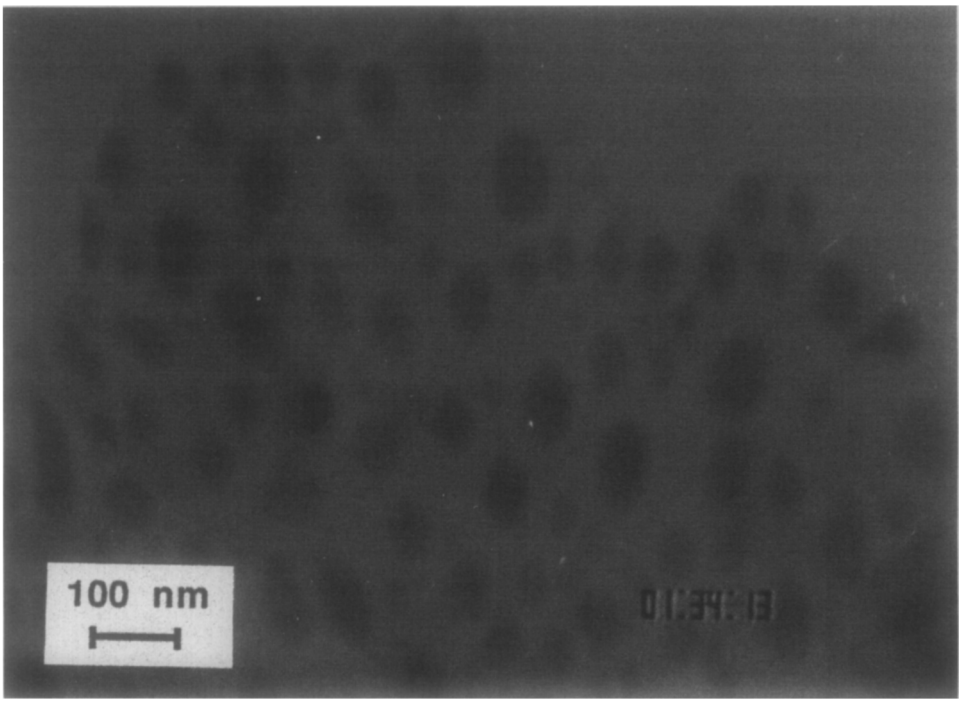

b

FIG. 4. CAEM images of $Sn(1–5)/Al_2O_3$ sample during heating in 2 Torr hydrogen. Specimen had been oxidized in a previous run. (a) At 713 K. Tin oxide particles visible. (b) At 762 K, 2.5 min later Particles have been reduced to metallic Sn.

opportunity to observe the behavior of metal particles on two different support media under identical reaction conditions. During initial heating in 3 Torr oxygen, the evaporated metal film collected into 20-nm particles on alumina and exhibited a small increase in average particle size on increasing the temperature to 925 K. On the graphite support, the tin formed into an interconnected structure of small particles and remained in this state upon heating to 925 K. The tin oxide network was not mobile during gasification, and no channeling or pitting action of the graphite by the tin oxide was observed. When specimens were cooled and reheated in 1 Torr hydrogen, particles present on alumina exhibited similar behavior to that reported above for the first series of CAEM experiments. At 870 K the network of oxide particles on graphite was observed to collapse into large globular particles of metallic tin. When the specimen was reheated in 3 Torr oxygen, the metal particles on graphite transformed into toroidal form at temperatures between 470 and 535 K, as shown in Fig. 5. Subsequent reduction/oxidation cycles showed that this change in morphology was reversible.

Supported Platinum–Tin Samples: TEM and STEM Studies

Pt–Sn/Al_2O_3 samples. A Pt–Sn/Al_2O_3 sample was prepared with a Pt : Sn atomic ratio of 1 : 1. This specimen contained discrete 5- to 20-nm-sized particles, as shown in Fig. 6a. The diffraction pattern, Fig. 6b, indicated that PtSn alloy (niggliite) has formed, and no other platinum or tin phase was present. This diffraction result is consistent with EDX data on individual parti-

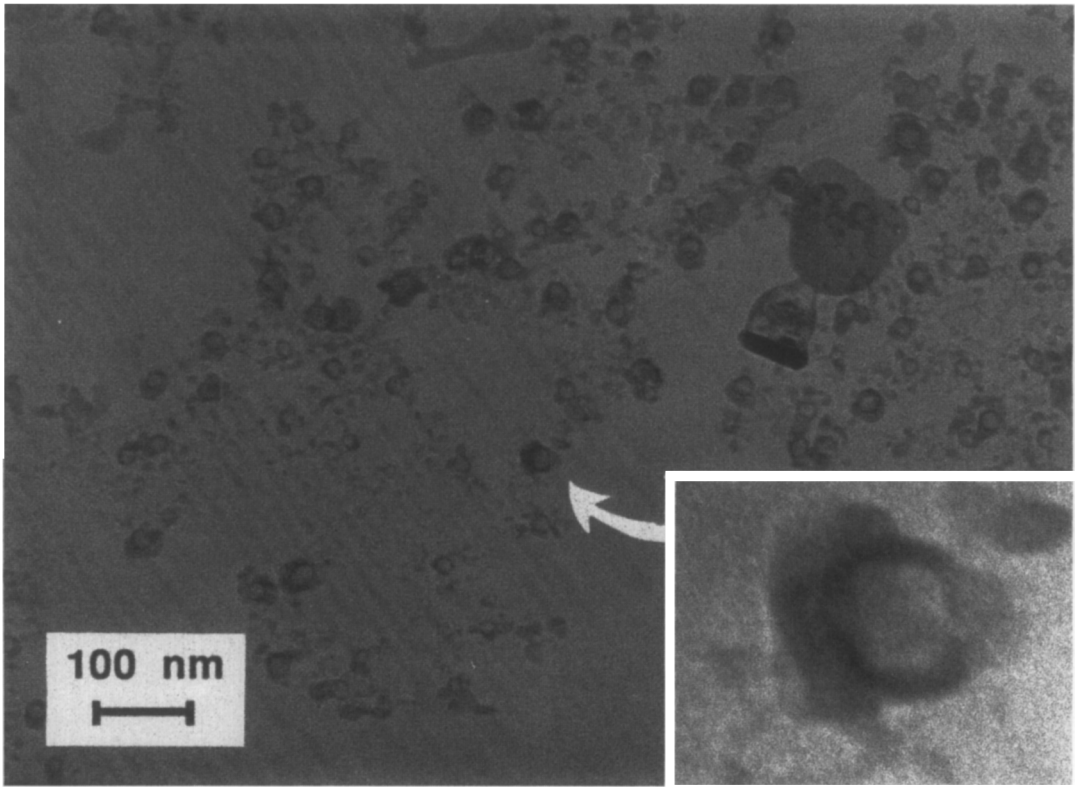

FIG. 5. CAEM image of Sn(1–5)/C region of mixed-support sample at 535 K in oxygen. Close-up shows tin oxide morphology.

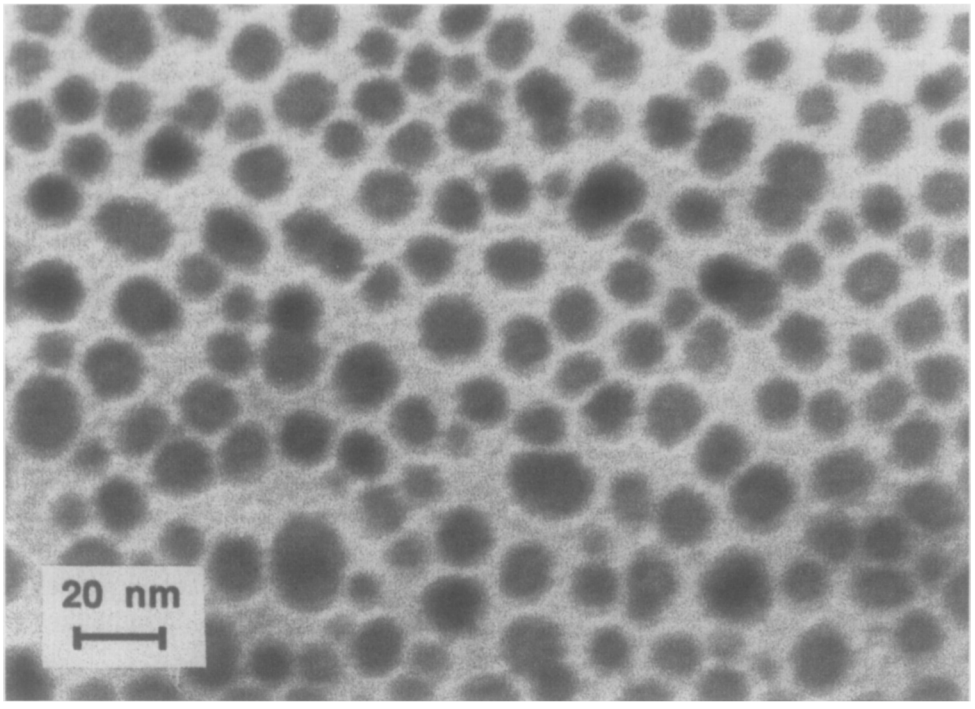

a

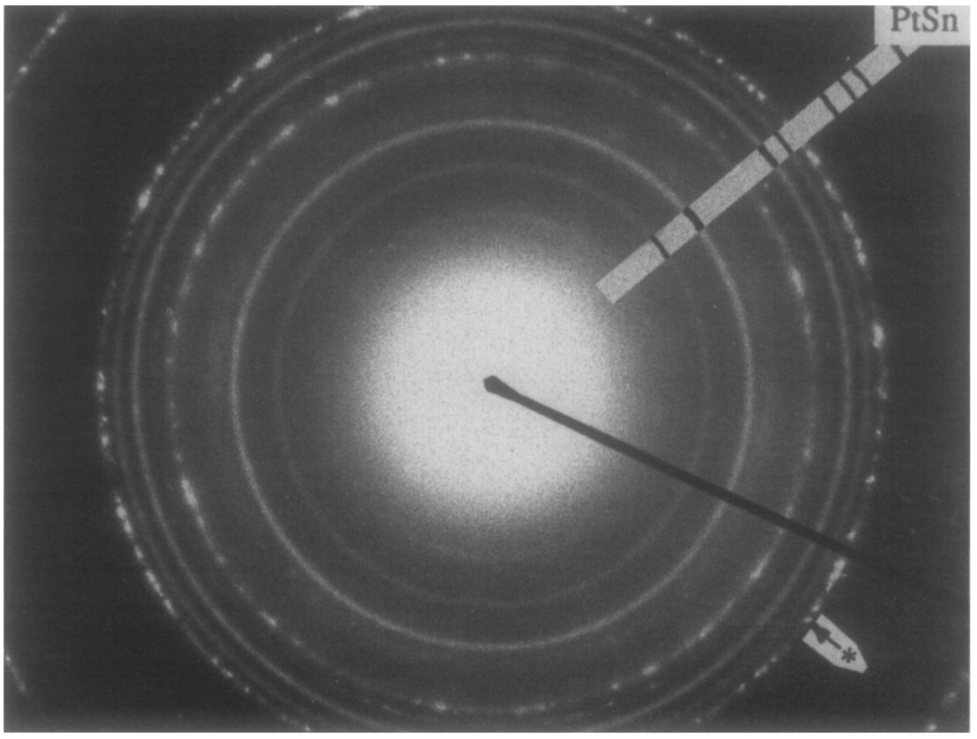

b

* = γ-Al_2O_3(400) line

FIG. 6. Pt–Sn(1 : 1)/Al_2O_3 sample after reduction in hydrogen at 770 K for 8 h. (a) Bright field image; (b) diffraction pattern.

TABLE 1

EDX Data from Reduced Pt–Sn(1 : 1)/Al_2O_3 Sample

No.	Feature	Counts (100 s)		Calculated[a] Pt/Sn at. ratio
		Pt	Sn	
1	Field at 200,000×	3237	3198	0.97
1a	Field at 200,000×	3237	3198	0.96
2a	20-nm particle	2332	2006	1.09
3a	10 nm away from above particle	25	23	1.05
4a	Another nonparticle area	72	53	1.30
5a	20-nm particle	2578	2413	1.01
6a	25-nm particle	1654	1490	1.05
7a	10-nm particle	679	789	0.82
8a	5-nm particle	318	301	1.01
9a	Another nonparticle area	7	6	1.16
10a	25-nm particle	1242	1161	1.02
11a	Replicate of 10a	1555	1436	1.03

Note. The count region energies were: Pt–$L\alpha$: 9.39–9.50 keV; Sn–$L\alpha$: 3.39–3.50 keV.

[a] Calculated using $K_{Sn-Pt} = 0.83 \pm 0.04$.

cles of the specimen. These EDX data are presented in Table 1, and show that the Pt/Sn atomic ratio is indeed unity for all individual particles analyzed. This sample will be denoted Pt–Sn(1 : 1)/Al_2O_3.

When the specimen was oxidized at 770 K, the particles assumed a core/shell appearance. These structures were analyzed by STEM, and they are shown in bright field in Fig. 7a. It was possible, through stopped beam mode and EDX analysis, to perform elemental mapping of selected particles. The EDX data tabulated in Table 2 show that the core regions of the particles are platinum-rich, whereas the peripheral regions are tin-rich. In addition, the X-ray yields from the core regions were notably higher than yields from the peripheral regions. Although this effect is due in part to increased beam broadening, especially if a feature containing mostly platinum is involved in the analysis area, it also indicates a thicker analysis region. This suggests that the peripheral material assumes a thinner

TABLE 2

EDX Data from Particles on Oxidized Pt–Sn(1 : 1)/Al_2O_3 Catalyst

No.	Feature	Counts (50 s)		Calculated[a] Pt/Sn at. ratio	Comments
		Pt–$L\alpha$	Sn–$L\alpha$		
1	Center of 20-nm particle	870	426	2.5	Pt-rich
2	Support	23	16	1.7	Low noise
3	10-nm particle, central core	1005	456	2.7	Pt-rich
4	Area next to 3, light apron region	230	350	0.8	Sn-rich
5	Center of 10-nm core/shell particle	2109	849	3.0	Pt-rich

Note. The count region energies were: Pt–$L\alpha$: 9.39–9.50 keV; Sn–$L\alpha$: 3.39–3.50 keV.

[a] Calculated using $K_{Sn-Pt} = 0.83 \pm .04$.

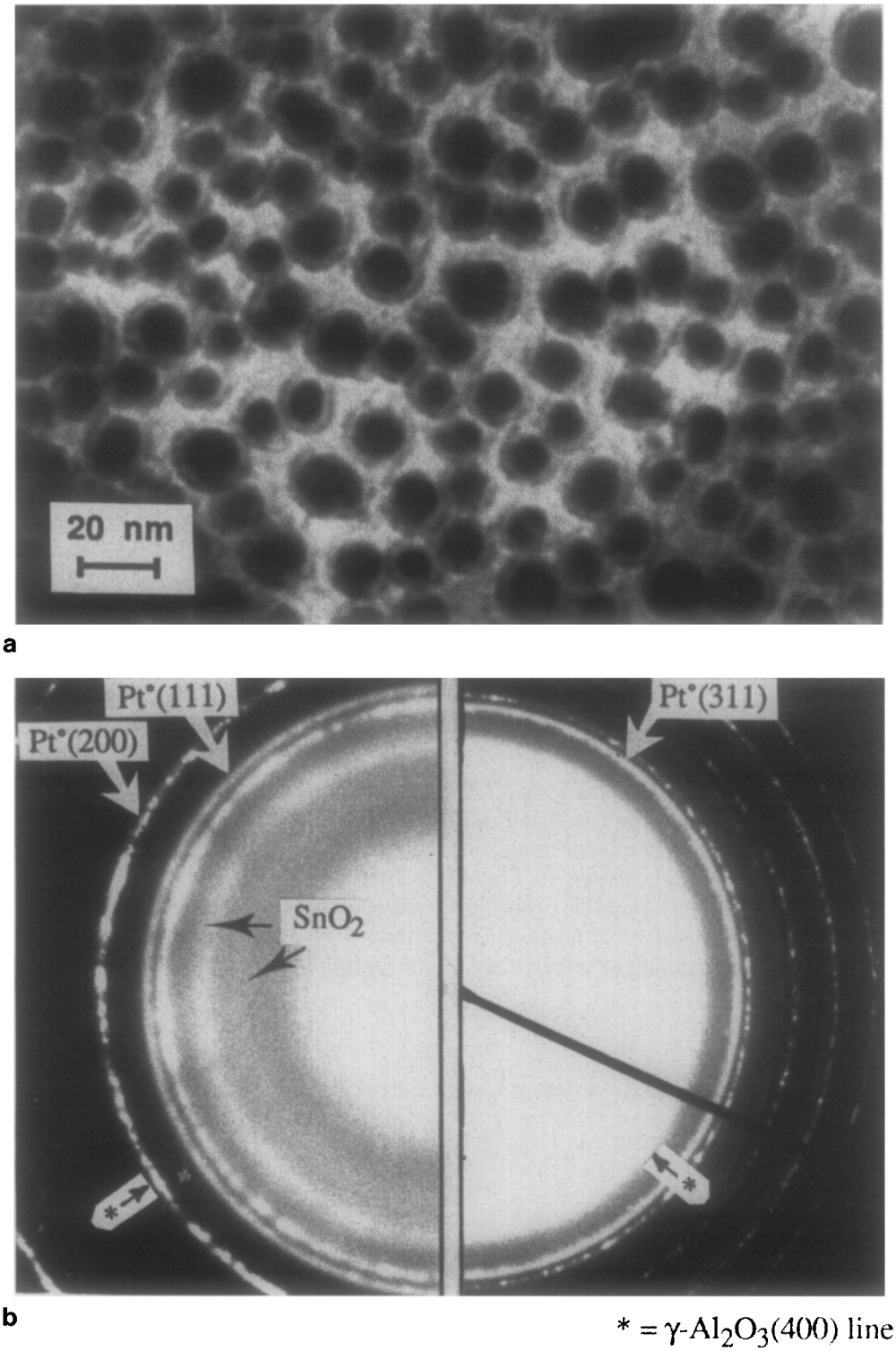

FIG. 7. Pt–Sn(1 : 1)/Al_2O_3 sample after treatment in oxygen at 770 K for 8 h. (a) Bright field image; (b) diffraction pattern. Pattern is displayed at two different camera lengths (note γ-Al_2O_3(400) location) to show SnO_2 lines.

profile than the core material. The selected area diffraction pattern of this specimen (Fig. 7b) showed that SnO_2 and metallic platinum phases were present. The SnO_2 is expected to wet the alumina surface to a greater extent than the platinum particles, and as a consequence it is expected to be the more thinly dispersed phase. In a final treatment step, the specimen was re-reduced at 770 K, and the particles assumed a more uniform contrast. The diffraction pattern showed that in this case only PtSn was present.

A second Pt–Sn/Al_2O_3 sample was prepared with a Pt : Sn atomic ratio of 0.5 : 1. This sample formed alloy particles after initial reduction at 770 K, as seen in Fig. 8a. The alloy phase detected by electron diffraction in this sample was found to be mostly $PtSn_2$ (Fig. 8b), with a small amount of PtSn. Energy dispersive X-ray data also support the diffraction evidence that the specimen has a greater amount of tin than platinum, since all particles analyzed registered a Pt/Sn ratio of less than unity, as shown in Table 3. The average Pt/Sn ratio was 0.5 ± 0.2. This sample will be denoted as Pt–Sn (0.5 : 1)/Al_2O_3.

Morphological changes accompanying oxidation and re-reduction were observed on the particles seen in Fig. 8a. The core/shell morphology was present in all particles following oxidation, as seen in Fig. 9a. While the overall particle outline has not changed appreciably in size, the central dark features have contracted upon oxidation. Lines corresponding to the strongest lines of SnO_2 and metallic platinum were

TABLE 3

EDX Data from Particles in Freshly Reduced Pt–Sn(0.5 : 1)/Al_2O_3 Catalyst

No.	Feature	Counts (50 s)		Calculated[a] Pt/Sn at. ratio
		Pt–$L\alpha$	Sn–$L\alpha$	
1	Blank support	82	101	0.98
2	15-nm particle	572	1157	0.60
3	Another 15-nm particle	120	228	0.63
4	Replicate of 3	414	1230	0.41
5	Replicate of 3	388	1158	0.40
6	Replicate of 3	590	1394	0.51
7	10-nm particle	597	1168	0.62
8	10-nm particle	527	939	0.68
9	Replicate of 8	579	992	0.70
10	Blank support	70	130	0.65
11	Replicate of 10	84	129	0.78
12	Replicate of 10	96	131	0.88
13	Blank support	78	146	0.64
14	25-nm particle	599	2423	0.30
15	5-nm particle	342	596	0.69
16	Blank support	97	143	0.82
17	25-nm particle	839	4061	0.25
18	30- to 35-nm particle	586	2651	0.27
19	10- to 15-nm particle	395	1601	0.30
20	5- to 10-nm particle	401	890	0.54
21	5-nm particle	239	442	0.65
22	5-nm particle	308	507	0.73

Note. EDX data on particles only: Pt/Sn = 0.53 ± 0.19. The count region energies were: Pt–$L\alpha$: 9.39–9.50 keV; Sn–$L\alpha$: 3.39–3.50 keV.

[a] Calculated using $L_{Sn-Pt} = 0.83 \pm 0.04$.

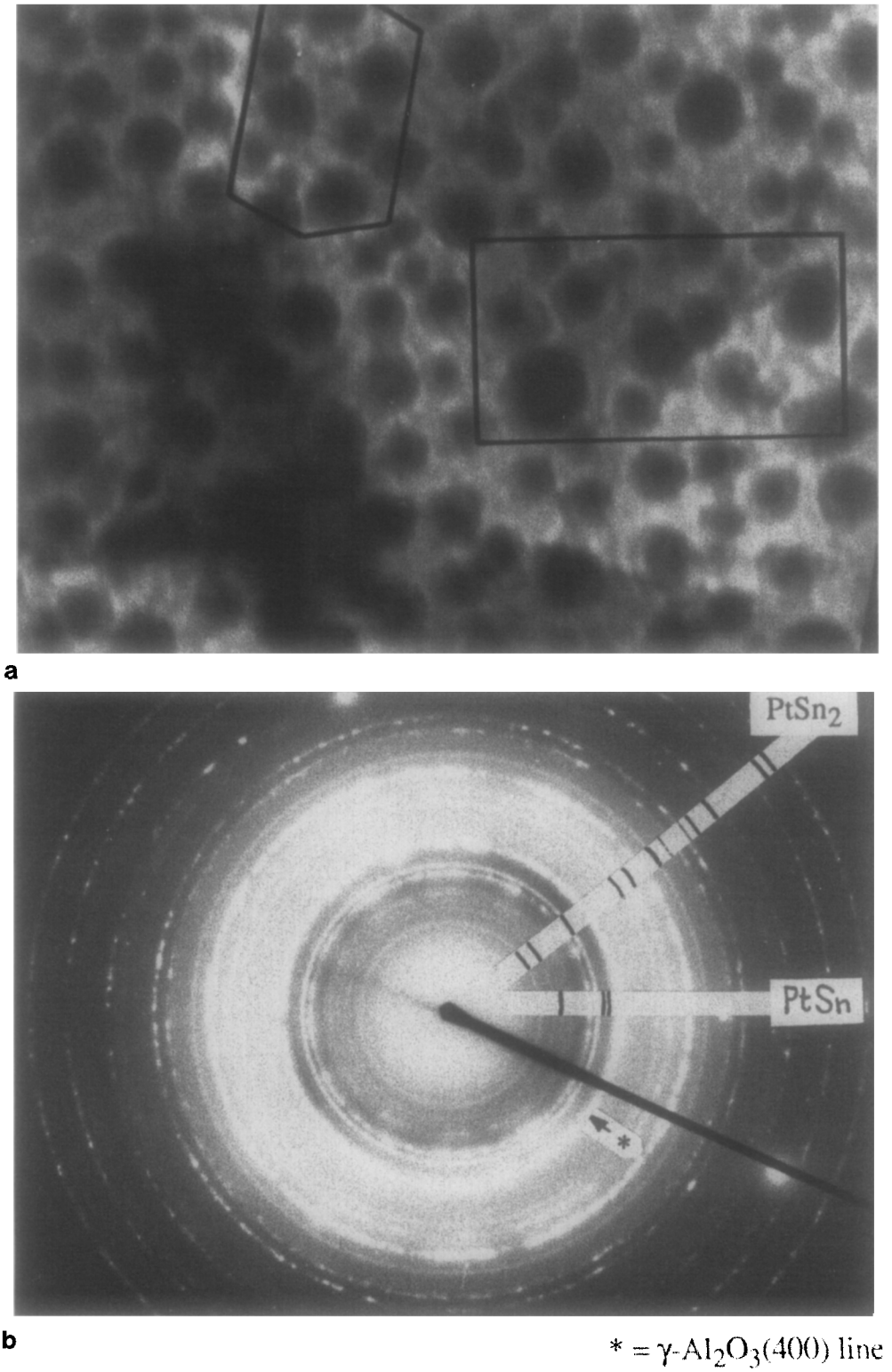

FIG. 8. Pt–Sn(0.5 : 1)/Al_2O_3 sample reduced in hydrogen at 770 K for 8 h. (a) Bright field image; (b) diffraction pattern.

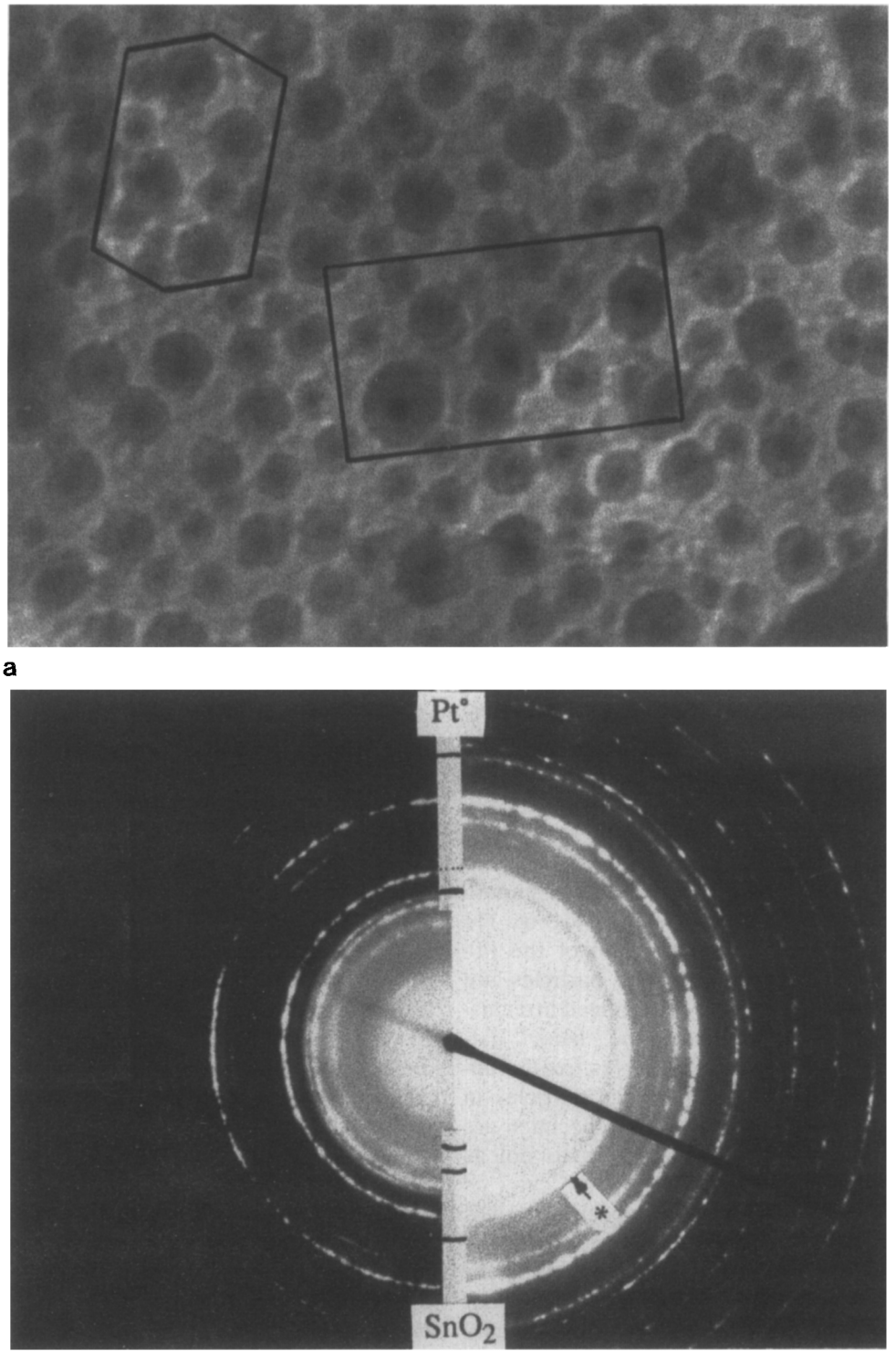

FIG. 9. Pt–Sn(0.5 : 1)/Al_2O_3 sample after treatment in oxygen at 770 K for 8 h. (a) Bright field image; (b) diffraction pattern.

seen in the diffraction pattern (Fig. 9b). Therefore, the dark features seen in the oxidized particles are probably platinum particles. When the specimen was re-reduced, at 770 K, the dark features expanded to cover most of the original particle field (see Fig. 10a). However, a thin layer is still visible on the periphery of each particle. In contrast to the diffraction data after the first reduction, in this case PtSn (niggliite) is detected as the only nonalumina phase that is present (see Fig. 10b). Therefore, some of the tin has been lost or rendered inaccessible to the platinum. The former possibility seems unlikely, in view of past observations by controlled atmosphere electron microscopy which failed to show tin loss. A more plausible explanation is that a tin oxide–alumina surface phase has formed, which is not subsequently reduced.

Pt–Sn/C catalysts. The reduction of Pt–Sn/C catalysts at 770 K leads to alloy formation. In the case of Pt–Sn(0.5 : 1)/C, the diffraction pattern (Fig. 11a) showed PtSn and $PtSn_2$ (*23*). The Pt–Sn(1 : 1)/C specimen (Fig. 11b) showed entirely PtSn. The results for the Pt–Sn/C specimens are consistent with what was seen with freshly reduced Pt–Sn/Al_2O_3.

The metal alloy particles on graphite are globular, uniformly contrasted, and smooth textured. The particles shown in Fig. 11c are from a basal plane region of the Pt–Sn(0.5 : 1)/C specimen. The particles are discrete and appear to be arranged in a cluster-like fashion, similar to the "lacey" pattern observed in Sn/C samples treated under oxidizing conditions. The particles in the more heavily loaded 1 : 1 specimen are larger, and the "lacey" pattern is not as evident.

The Pt–Sn(0.5 : 1)/C specimen was heated in oxygen to 770 K for 8 h, along with a Pt(1)/C specimen. The results for both samples are shown in Fig. 12. Platinum is known to catalyze graphite gasification, creating channels across the basal plane surfaces (*24*). This behavior is apparent in Fig. 12a, a micrograph having been taken from a region near a graphite edge. The diffraction pattern showed the existence of metallic platinum. In contrast, the edge regions of the Pt–Sn(0.5 : 1)/C specimen showed few channels (Fig. 12b), and very few of the particles could be associated with channeling or pitting action. The individual particles had transformed into a core/shell morphology. The diffraction pattern identified metallic platinum and SnO_2 phases. As was determined for the Pt–Sn/Al_2O_3 samples under oxidizing conditions, the platinum is associated with the dark features, usually centrally located in the particles, with SnO_2 being the lighter contrasted rough-textured, surrounding material.

DISCUSSION

Supported Tin Samples

The tin deposition process produced discrete particles on the substrates. When heated in hydrogen at 770 K, the tin coalesced into spherically shaped metal particles. This is consistent with the nonwetting behavior resulting from the weak interaction between metal crystallite and support, such as has been reported for other cases of noninteracting metals on supports (*25*).

When metallic tin particles are treated in oxygen at 770 K, increased wetting of the substrate is expected to occur since the surface tensions of metal oxides are lower than those in metals. Furthermore, if the crystallite–substrate interaction energy produced by the oxide–oxide interaction is sufficiently favorable, then the crystallite–substrate interfacial tension will be lowered and crystallite spreading may occur.

Sn/Al_2O_3 Catalysts

In the reduced, low-loading Sn/Al_2O_3 specimens, the core/shell morphology is prevalent. The thin peripheral phase is oxidized tin. A bulk tin oxide phase (i.e., SnO or SnO_2) could be responsible for the thin apron surrounding the metallic tin central core; however, as bulk phases, these oxides would be reduced during hydrogen

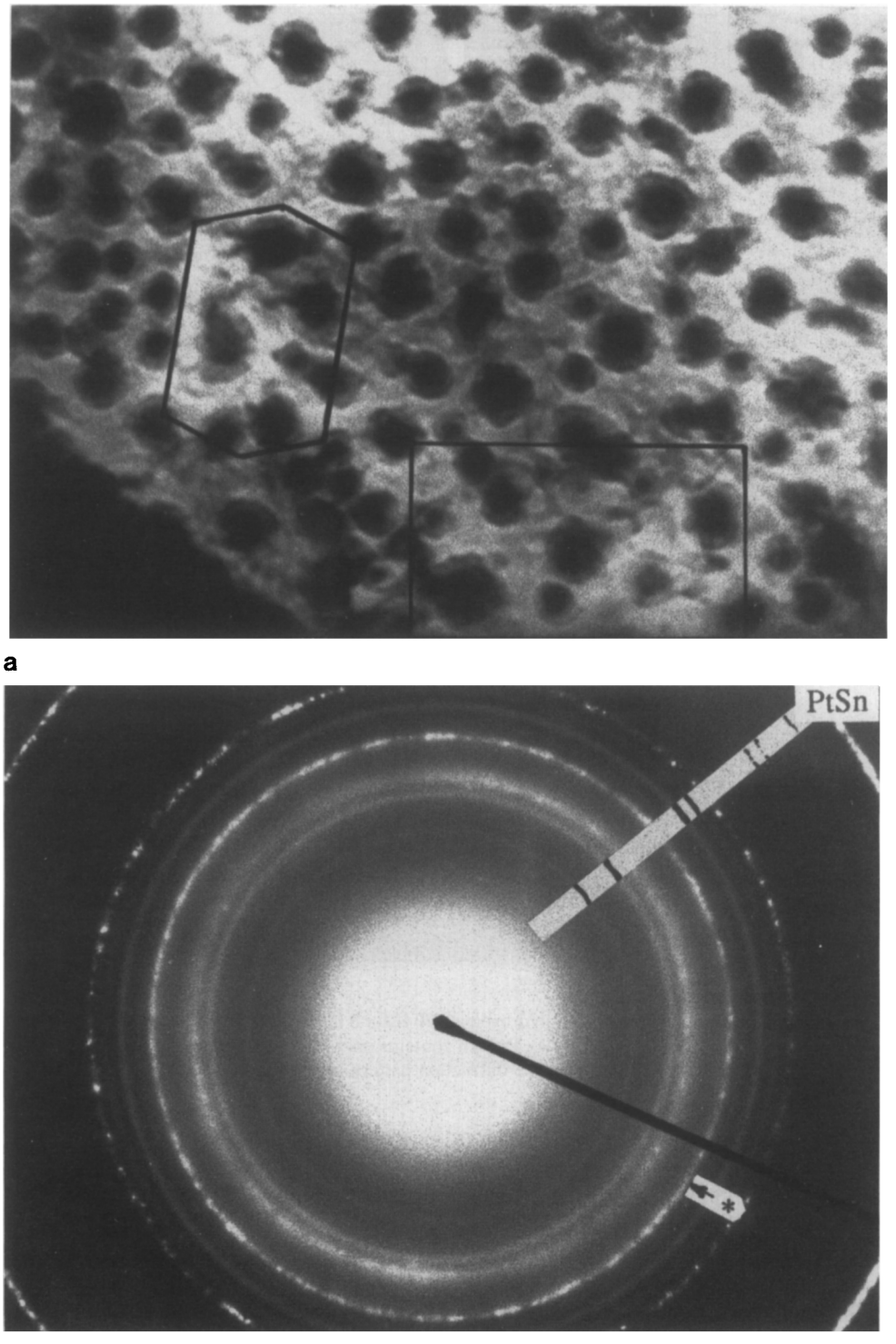

FIG. 10. Pt–Sn(0.5 : 1)/Al_2O_3 sample re-reduced in hydrogen at 770 K for 8 h. (a) Bright field image; (b) diffraction pattern.

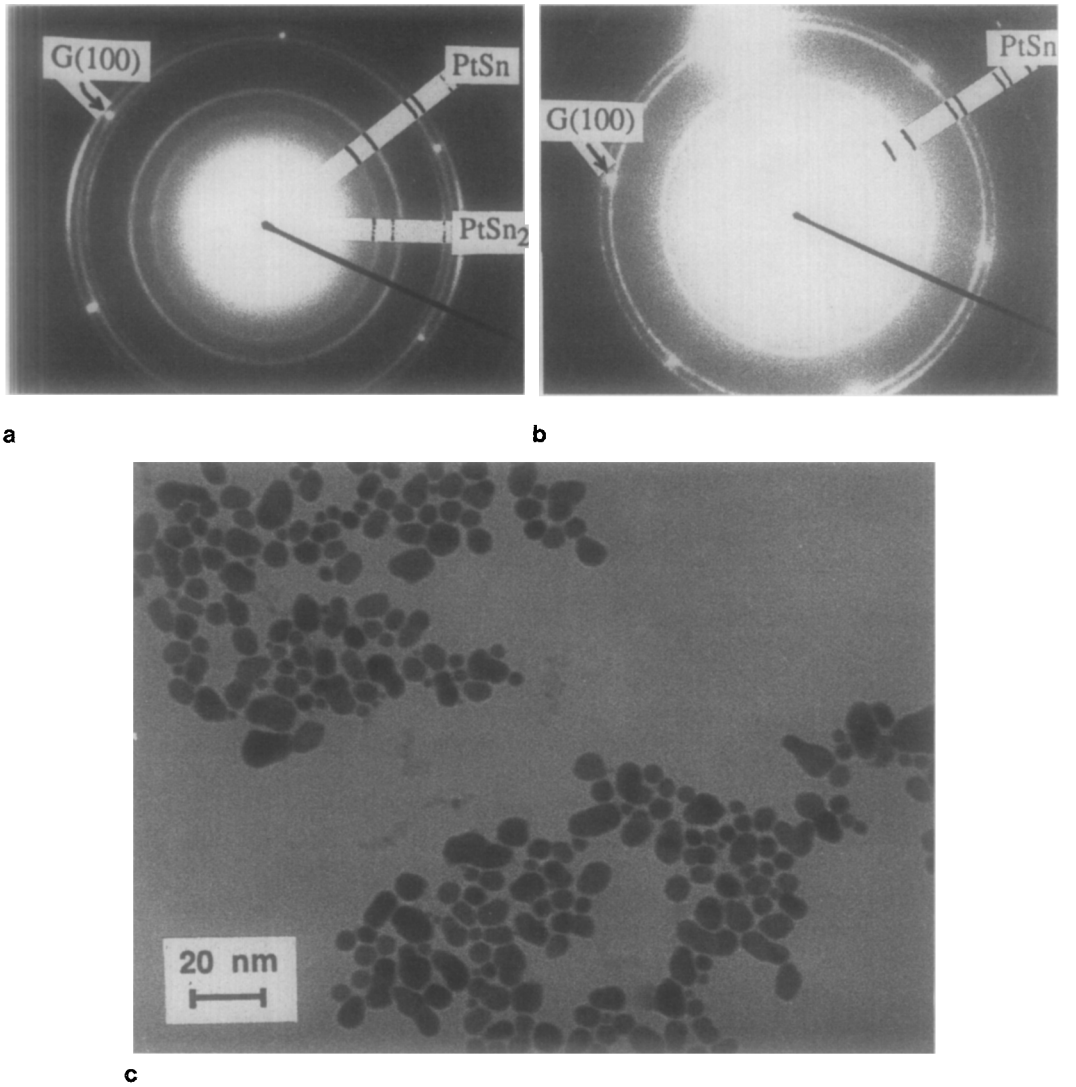

FIG. 11. Pt–Sn/C sample reduced in hydrogen at 770 K for 8 h. (a) Pt–Sn(0.5 : 1)/C. Pattern shows a small amount of $PtSn_2$. (b) Pt–Sn(1 : 1)/C. Pattern contains only PtSn (niggliite). (c) Bright field image of Pt–Sn(0.5 : 1)/C. The "G" indicates the diffraction pattern of graphite.

treatment. Alternatively, a tin (II) aluminate phase may be the thin oxide layer. Bulk tin aluminate is a spinel structure and normally forms at temperatures greater than 1873 K (*20*). A limited migration of stannous ions into the defect structure of γ-phase alumina could be favorable at lower temperatures. Indeed, the stabilization of oxidized tin species on alumina has been reported (e.g., Refs. (*2–7*)).

The toroidal-shaped oxide particles observed on oxidized Sn/Al_2O_3 samples may be envisaged as a stable morphology under the oxidizing environment or as a consequence of rapid nonequilibrium spreading. From a thermodynamic viewpoint, one would expect a droplet-shaped particle to represent the most stable energetic configuration, since for the same amount of crystallite material, a toroidal structure has a

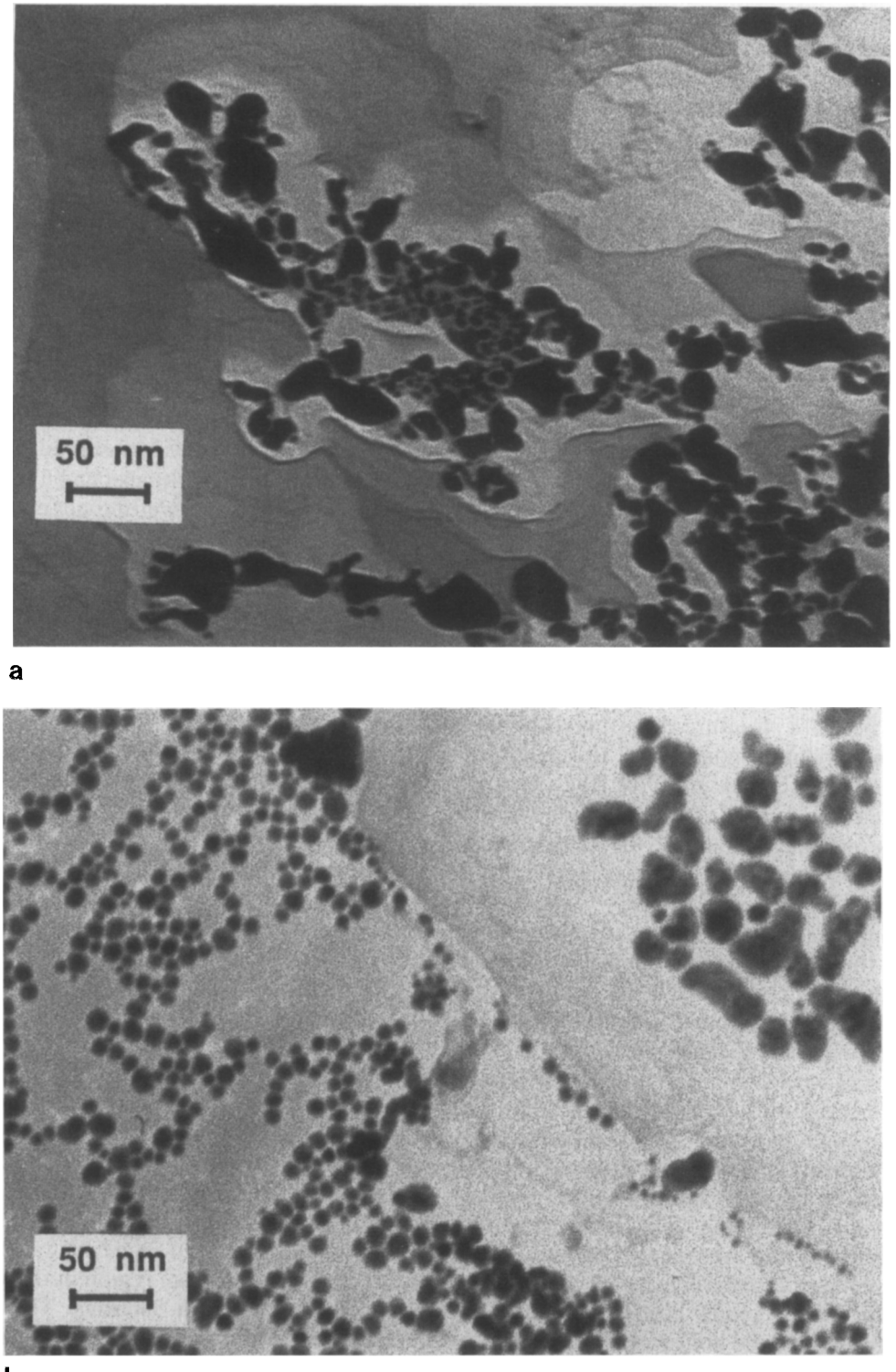

FIG. 12. Comparison of oxidized Pt(1)/C and Pt–Sn(0.5 : 1)/C samples. (a) Pt(1)/C; (b) Pt–Sn (0.5 : 1)/C.

higher surface/volume ratio. However, if the surface tension near the central area in a torus is lower than the substrate surface tension, due to formation of a strongly interacting oxide–support phase in this open area, then a torus could be stabilized (*26*). In addition, the appearance of this morphology as a consequence of rapid (nonequilibrium) spreading was discussed by Ruckenstein and Sushumna (*27*) for Fe/Al_2O_3 under oxidation conditions. The larger tin particles on oxidized Sn/Al_2O_3 samples did not become toroidally shaped. If the spreading is slower for these particles, the toroidal morphology would not be realized.

Sn/C Catalysts

On the chemically more inert graphite basal plane surface, deposits of metallic tin coalesced into round particles upon treatment in hydrogen at 770 K, while the transformation was slower for smaller tin deposits which exhibited a network structure. The network structure corresponds to SnO_2 under oxidation conditions. In CAEM experiments, coalescence of the network structure upon reduction into globular metallic particles occurs at the same time as large SnO_2 toroidal particles become uniformly contrasted. The SnO_2/C interaction is apparently quite strong, in view of the fact that tin oxide reduction is already thermodynamically feasible at temperatures slightly above ambient. The transformation of round, metallic Sn particles into SnO_2 toroidal particles is seen in dynamic studies at temperatures between 500–600 K. The rapid spreading under these conditions may be a result of the sudden transformation from a liquid, nonwetting particle to a more strongly interacting solid phase and also perhaps by the presence of oxygen on the graphite. Alternatively, the apparent toroidally shaped oxide particles on graphite could actually be hollow spheres formed by the diffusion of tin to the surface of the oxide particle during oxidation (*28*). In contrast, the formation of toroidal particles upon oxidation of Sn/Al_2O_3 is more gradual in comparison to Sn/C, indicative of stronger interactions of tin with Al_2O_3.

The gasification of graphite is catalyzed by a number of metals and metal oxides (*29, 30*), and this reaction is believed to occur by an oxygen-transfer mechanism in which the active catalysts serve as oxygen carriers to the graphite surface by undergo a redox cycle. The results presented here are consistent with data reported by McKee (*30*) who found no evidence for catalytic attack by either tin or tin oxide. Specifically, no edge recession, channeling, or pitting of the graphite basal plane in the vicinity of the particles was observed in this study. These modes of attack can be related to the interaction and wetting characteristics of the catalyst (31). In the case of metal oxides, the particles undergo a strong attraction to the oxygenated graphite edge and step sites. The interfacial attraction causes spreading along the edges to form a thin layer, and in this way the edge recession can be expedited catalytically. However, to perform the redox cycle necessary for oxygen transfer, the metal oxide must be at least partially reducible by the graphite in the oxygen environment (*30*). In the case of tin, it appears that the SnO_2 formed is too stable to allow this reaction to occur. In this respect, the behavior of tin would coincide with that of Fe and Ni, both of which readily form stable oxide phases that are apparently not amenable to partial reduction by graphite.

The results of this study indicate that metallic tin particles interact weakly with alumina and graphite supports. The primary difference between the behavior of the metal on these two supports under reducing conditions is that a fraction of the tin remains in an oxidized state on alumina, forming a tin–aluminate region in the vicinity of the metallic tin particles. This phenomenon serves to anchor the metallic tin particles on the surface, thereby leading to greater resistance to sintering of tin on alumina compared to graphite.

In contrast to metallic tin, tin oxide interacts more strongly with alumina and graphite supports. This interaction is manifested as a spreading action of tin oxide over the support surface during oxidation treatments, leading to the formation of toroidal-shaped particles. Furthermore, evidence for the existence of tin oxide/support interactions is provided by the observation that temperatures near 760 K in hydrogen were required to convert the toroidally shaped particles to the round particles characteristic of metallic tin. The stabilization of tin oxide on alumina is most likely due to formation of Sn–O–Al linkages, whereas the interaction of tin oxide with graphite may be due to bonding of tin with carbon oxide moieties at defect sites on the support.

Supported Pt–Sn Samples

The sequence of Pt–Sn particle morphologies at each treatment stage is depicted schematically in Fig. 13 for the Pt–Sn/Al_2O_3 specimens. Before treatment, the freshly prepared catalysts are speculated to consist of a metallic tin particulate phase with a platinum film overlayer (since Pt was the second metal deposited). Heating in hydrogen to 770 K resulted in the formation of discrete alloy particles. The composition of the alloy formed varied with the relative amounts of metal deposited. When the alloy particles were treated in oxygen at 770 K, tin oxide (SnO_2) formed an external layer, giving the particle a core/shell morphology, due to the higher electron scattering amplitude of the platinum compared to tin. Rereduction of the specimens led to Pt–Sn alloy formation in both 0.5 : 1 and 1 : 1 specimens. The formation of PtSn in the Pt–Sn (0.5 : 1)/Al_2O_3 specimen, rather than $PtSn_2$, indicates a loss of reducible tin to the support as a dispersed, oxide layer. Comparison of Figs. 9 and 10 for the Pt–Sn (0.5 : 1)/Al_2O_3 sample shows that the dark cores of the oxidized particles have grown with re-reduction, although they do not completely encompass the entire particle perimeter.

On the graphite support, the alloy particles formed are globular and uniformly contrasted. Upon oxidation, the core/shell morphology is seen, similar to the structures shown in Fig. 13 for Pt–Sn/Al_2O_3, but without formation of a tin oxide–support phase. The ability of SnO_2 to wet the graphite basal plane was demonstrated by the rapid transformations of uniformly con-

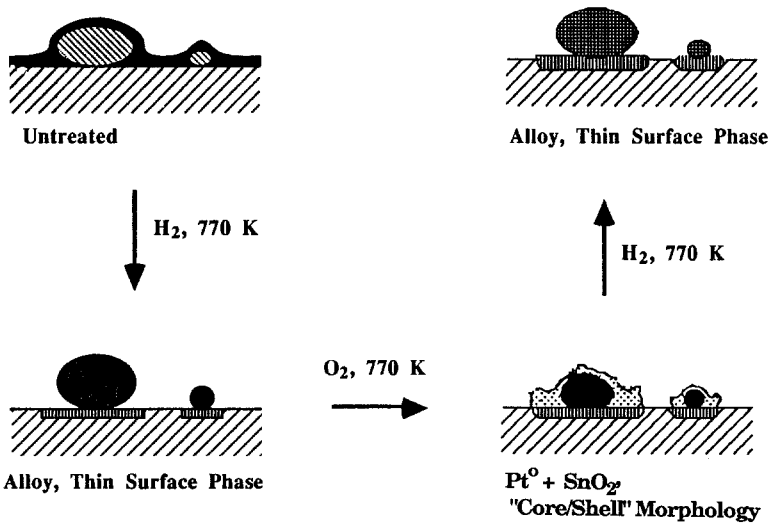

FIG. 13. Schematic of particle transformations in Pt–Sn/Al_2O_3.

trasted metallic tin particles to oxide torus structures, seen in controlled atmosphere electron microscopy studies of Sn/C specimens described earlier.

The results of this study show that a distinct particle morphology can be identified with segregation of the platinum and tin under oxidation conditions, and, provided that a sufficient amount of platinum is present, the tin may be retrieved for alloying upon re-reduction at 770 K. This result is in agreement with the recent study by Gardner *et al.* (32) who showed that Pt/Sn alloy particles form upon reduction of Pt/SnO_2 at 720 K. The preferential oxidation of tin in Pt–Sn alloy particles results in a local segregation of the metals. A similar result was observed by Wang and Schmidt (*21, 22*) for Pt–Rh particles supported on silica thin films. The oxide Rh_2O_3 wets the support surface and, upon reduction, fragments into small Rh crystallites.

For the Pt–Sn system, it is doubtful that re-dispersed Sn particles could be created by oxidation/reduction, because SnO_2 is not readily reducible. It has been shown in controlled atmosphere electron microscopy experiments that tin is oxidized at temperatures as low as 520 K, whereas reduction takes place at 850 K on both alumina and graphite. This suggests that Pt facilitates the reduction of SnO_2 to form Pt–Sn alloy particles. On $Pt–Sn(0.5:1)/Al_2O_3$, a thin oxide phase was visible in the re-reduced catalyst. Reduction of this oxide layer would require a temperature higher than 770 K, and this would probably result in coalescence of Sn particles with the parent particle. The $Pt–Sn(1:1)/Al_2O_3$ specimen showed reversible formation of an alloy phase. This re-reduction process was not completely reversible for the $Pt–Sn(0.5:1)/Al_2O_3$ sample.

The inhibiting influence of tin on platinum catalytic activity is apparent by the absence of catalytic carbon gasification in the graphite-supported Pt–Sn specimens under oxidation conditions. The gasification of graphite by Pt has been studied previously by electron microscopy (*24*). The reaction occurs preferentially at steps, edges, and other surface defect structures in the basal plane, and this reaction is promoted by the presence of metals and metal oxides at such surface features. The lack of channeling action in the Pt–Sn/C system, compared to Pt/C, indicates a suppression of Pt-catalyzed gasification. This behavior is consistent with the notion that tin oxide preferentially segregates to the graphite interface and forms a protective layer. The core/shell Pt–Sn particle morphology shows that the platinum crystallite is physically isolated from the graphite by a layer of tin oxide. Thus, there is no Pt/C interface at which carbon may be oxidized by oxygen activated on platinum sites. It is interesting to contrast the behavior of Pt–Sn particles with the behavior of Pt–Ir and Pt–Rh particles (*33, 34*), where the metals are considered to remain as alloys, with surfaces enriched in iridium and rhodium, respectively. Channeling by these particles was possible because metal oxide formation was incomplete, and there was sufficient mobility in the surface layer to facilitate diffusion of carbon to metal sites.

Alloy particles of composition Pt_3Sn and PtSn have been shown by Dautzenberg *et al.* (*2*) to be active for *n*-hexane reactions at temperatures near 720–820 K. Despite the fact that Sn(II) may be the predominant tin species in reduced Pt–Sn-reforming catalysts, it is still possible for a small amount of alloyed tin to modify the platinum catalytic function. In general, the type and extent of tin phases present will be dependent upon metal loading, treatment temperature, and the presence of species such as chlorine, which play an important role in the redispersion of platinum. Physical structures proposed previously in the literature (*4, 7*) depict "patches" of platinum and tin highly associated, and a thin film of tin aluminate phase that does not reduce below Sn(II). The core/shell morphology ob-

served on the $Pt–Sn/Al_2O_3$ model catalysts of the present study is consistent with this description.

In summary, it is suggested that the behavior of the model supported $Pt–Sn/Al_2O_3$ samples of the present study may mimic the performance of high-surface-area $Pt–Sn/Al_2O_3$ catalysts where the metal loading is rather high. At lower metal loadings, all of the tin may be stabilized in an oxidic state on the alumina surface, and Pt–Sn alloy particles may not be present in significant quantity.

CONCLUSIONS

Tin on alumina can be reversibly converted between metallic tin and tin oxide at or below 770 K in particles larger than 20 nm. High-resolution TEM revealed the appearance of a core/shell morphology in reduced particles less than 20 nm in size. This is interpreted as showing the coexistence of a three-dimensional metallic crystallite with a thin, nonreducible surface tin oxide–support phase that results from surface reaction between oxidic tin and γ-Al_2O_3. In a reducing environment, the metallic particles are globular and exhibit poor wetting characteristics with the support. Oxidation of the particles results in particle spreading. In the smaller particles, transformation into toroidal configurations results during oxidation. On graphite, oxidic tin (SnO_2) appears to wet the basal plane of graphite, as evidenced under oxygen atmosphere by an immobile network structure of freshly prepared specimens, and by the toroidal structures formed from metallic tin spheres; however, the interaction of tin oxide with graphite appears to be weaker than with Al_2O_3. The tin oxide was not active for catalytic gasification of graphite, due to its inability to undergo redox processes under reaction conditions.

Alloy formation occurs in monolayer depositions of platinum and tin upon reduction at 770 K. Oxidation at this temperature segregates the two metals into metallic platinum and tin(IV) oxide, the latter of which wets the support. Rereduction at 770 K reforms an alloy, with platinum facilitating the reduction of SnO_2. The graphite substrate is more weakly interacting with tin than the alumina substrate. In the case of alumina-supported catalysts, some of the tin reacts with the alumina to form a tin oxide surface phase that is not easily rereduced to the metallic state, and, depending upon the amount of platinum present, a portion of the tin remains on the support as a surface oxide phase.

ACKNOWLEDGMENTS

We acknowledge the donors of the Petroleum Research Fund, administered by the American Chemical Society, for the partial support of this research. We also thank Sanjay Sharma and Randy Cortright for invaluable contributions during the latter stages of this work, and we thank Professor Stanley Langer for his encouragement during the entire project.

REFERENCES

1. Davies, E. E., Elkins, J. S., and Pitkethly, R. Ch., US Patent 3,759,823 (1971); also Dautzenberg, F. M., German Offen. 2,121,765 (1971); Box, E. O., Drehman, L. E., and Farha, F., German Offen. 2,127,353 (1971); Wilhelm, F. C. (UOP) US Patent 3,844,938 (1974).
2. Dautzenberg, F. M., Helle, J. N., Biloen, P., and Sachtler, W. M. H., *J. Catal.* **63,** 119 (1980).
3. Bacaud, R., Bussière, P., and Figueras, F., *J. Catal.* **69,** 399 (1981).
4. Lieske, H., and Völter, J., *J. Catal.* **90,** 96 (1984).
5. Burch, R., *J. Catal.* **71,** 348 (1981).
6. Sexton, B. A., Hughes, A. E., and Foger, K., *J. Catal.* **88,** 466 (1984).
7. Adkins, S. R., and Davis, B. H., *J. Catal.* **89,** 371 (1984).
8. Kuznetsov, V. I., Belyi, A. S., Yurchenko, E. N., Smolikov, M. A., Protasova, M. T., Zatolokina, E. V., and Duplyakin, V. K., *J. Catal.* **99,** 159 (1986).
9. Gray, P. R., and Farha, F. E., "Mössbauer Effect Methodology," Vol. 10, p. 47. Plenum, New York, 1976.
10. Berndt, H., Mehner, H., Völter, J., and Meisel, W., *Z. Anorg. Allg. Chem.* **429,** 47 (1977).
11. Kuznetsov, V. I., Yurchenko, E. N., Belyi, A. S., Zatolokina, E. V., Smolikov, M. A., and Duplyakin, V.K., *React. Kinet. Catal. Lett.* **21:**(3), 419 (1982).
12. Muller, A. C., Engelhard, P. A., and Weisang, J. E., *J. Catal.* **56,** 65 (1979).

13. Srinivasan, R., De Angelis, R., and Davis, B. R., *J. Catal.* **106,** 449 (1987).
14. Qiao, G. W., Zhou, J., and Kuo, K. H., *in* "Proceedings, 8th International Congress on Catalysis, Berlin, 1984," Vol. 3, p. 93, Dechema, Frankfurt-am-Main, 1984.
15. Cocke, D. L., Johnson, E. D., and Merril, R. P., *Catal. Rev.* **26,** 163 (1984).
16. Ruckenstein, E., and Malhotra, M. L., *J. Catal.* **41,** 303 (1976).
17. Baker, R. T. K., and Sherwood, R. D., in "Microbeam Analysis—1986" (A. D. Romig and W. F. Chambers, Eds.), p. 317. San Francisco Press, San Francisco, 1986.
18. Asbury, D. A., and Hoflund, G. B., *J. Vac. Sci. Technol. A* **5,** 1132 (1987).
19. Mantell, C. L., *in* "Tin: Its Mining, Production, Technology, and Applications." Hafner Publishing, New York, 1970.
20. Spandau, H., and Ullrich, T., *Z. Anorg. Chem.* **274,** 271 (1953).
21. Wang, T., and Schmidt, L. D., *J. Catal.* **70,** 187 (1981).
22. Wang, T., and Schmidt, L. D., *J. Catal.* **71,** 411 (1981).
23. Wallbaum, H. J., *Z. Metallkd.* **35,** 200 (1943).
24. Baker, R. T. K., France, J. A., Rouse, L., and Waite, R. J., *J. Catal.* **41,** 22 (1976).
25. Baker, R. T. K., Thomas, C., and Thomas, R. B., *J. Catal.* **38,** 510 (1975).
26. Ruckenstein, E., *in* "Metal–Support Interactions in Catalysis, Sintering and Redispersion" (S. A. Stevenson, J. A. Dumesic, R. T. K. Baker, and E. Ruckenstein, Eds.), p 230. Van Nostrand–Reinhold, New York, 1987.
27. Ruckenstein, E., and Sushumna, I., *J. Catal.* **97,** 1 (1986).
28. Chen, A. A., Vannice, M. A., and Phillips, J., *J. Catal.* **116,** 568 (1989).
29. McKee, D. W., *in* "Chemistry and Physics of Carbon" (P. J. Walker, Jr. and P. A. Thrower, Eds.), Vol. 16. Dekker, New York, 1965.
30. McKee, D. W., *Carbon* **8,** 623 (1970).
31. Baker, R. T. K., *Carbon* **24**(6), 715 (1986).
32. Gardner, S. D., Hoflund, G. B., Davidson, M. R., and Schryer, D. R., *J. Catal.* **115,** 132 (1989).
33. Baker, R. T. K., Sherwood, R. D., and Dumesic, J. A., *J. Catal.* **66,** 56 (1980).
34. Baker, R. T. K., Sherwood, R. D., and Dumesic, J. A., *J. Catal.* **62,** 221 (1980).